Int J Thermophys (2009) 30:919–933
DOI 10.1007/s10765-009-0577-3

Molecular Dynamics Study on the Anisotropic Thermal Conductivity of Helium–Xenon Binary Nanocrystal Superlattices

Dan Bai

Received: 27 March 2008 / Accepted: 13 March 2009 / Published online: 2 April 2009

Abstract The anisotropic thermal conductivity of helium–xenon binary nanocrystal superlattices (BNSLs), which are stoichiometric solid structures $Xe(He)_2$ and $Xe(He)_{13}$, at high pressure and room temperature ($T = 300\,K$), respectively, has been calculated by equilibrium molecular dynamics (EMD) simulation using the Green–Kubo formalism and the exponential-6 intermolecular potential under periodic boundary conditions (PBC). The pressures obtained from EMD agree very well with those from an independent study, to within 5 %. Nonequilibrium molecular dynamics (NEMD) simulation is also carried out for comparison. The thermal conductivities predicted by NEMD are of the same order of magnitude as the results predicted by EMD. The anisotropic thermal conductivities of stoichiometric solid structures ($Xe(He)_2$ and $Xe(He)_{13}$) with different molar volume and atomic number are investigated, and results show that the thermal conductivities of $Xe(He)_2$ are more strongly anisotropic than those of $Xe(He)_{13}$, whereas the averaged thermal conductivities of $Xe(He)_2$ are around one tenth (1/10) of those of $Xe(He)_{13}$, indicating that the thermal conductivities of helium–xenon BNSLs ($Xe(He)_2$ and $Xe(He)_{13}$) significantly depend on the molecular structure in both magnitude and anisotropy. The results also show that both the magnitude and anisotropy of the thermal conductivity of helium–xenon BNSLs ($Xe(He)_2$ and $Xe(He)_{13}$) slightly depend on the atomic number and molar volume of the simulation system, with finite-size effects existing in the nanoscale system.

Keywords Anisotropic thermal conductivity · Binary nanocrystal superlattices · Helium–xenon mixtures · Molecular dynamics simulation

D. Bai (✉)
1011 Research Institute, School of Mechanical Engineering, Shanghai Jiaotong University,
1954 Hua Shan Road, Shanghai 200030, People's Republic of China
e-mail: bdsjtuucla@gmail.com; baidan@sjtu.edu.cn

1 Introduction

Studies have shown that mixtures of some microspheres (natural and synthetic) with selected size ratios can co-crystallize into binary AB, AB_2, AB_5, or AB_{13} nanocrystal superlattices [1–6]. These binary nanocrystal superlattices (BNSLs) have attracted considerable attention, as they can produce structures that are more complex than the standard hexagonal close-packed (HCP) and face-centered cubic (FCC) arrangements most frequently observed for single-component systems, moreover, as binary superlattices have the potential to create new "metamaterials" which display unique collective properties that differ from their individual components [6]. In addition, the thermal conductivity is a crucial thermodynamic parameter of the material, but "One of the most difficult transport coefficients to calculate has proven to be thermal conductivity [7]." So it is essential to investigate and understand the thermal conductivity of BNSLs.

The primary objective of this article is the study of the effect of various factors on the anisotropic thermal conductivity of BNSLs, e.g., the molecular structure, atomic number, and molar volume. Since the intermolecular potential of helium–xenon BNSLs ($Xe(He)_2$ and $Xe(He)_{13}$) can be obtained from Ref. [8], they have been studied as representations of BNSLs using molecular dynamics (MD) simulation. Previous research has known that MD is a viable method for providing insight into the nanoscale world, especially where thermal transport is concerned. Depending on the size and state of the system, as well as how well the underlying physics are understood, MD can provide the necessary properties of materials, such as thermal conductivity.

The thermal conductivity can be computed using equilibrium molecular dynamics (EMD) with Green–Kubo (EMD-GK) or nonequilibrium molecular dynamics (NEMD) simulation, which are two common MD approaches. One of the advantages of EMD-GK simulation over the NEMD simulation is the ability to compute the entire thermal-conductivity tensor in a single simulation enabling observers to capture the anisotropy of the system [9]. So this article employs EMD-GK simulation to study the anisotropic thermal conductivity of helium–xenon BNSLs ($Xe(He)_2$ and $Xe(He)_{13}$). Further information about EMD-GK and NEMD simulation is described in detail in Refs. [9–11].

2 EMD-GK Method and Simulation Conditions

In this article, EMD employs the Green–Kubo method to calculate the thermal conductivity of the stoichiometric solid structures, $Xe(He)_2$ and $Xe(He)_{13}$, at high pressure and room temperature ($T = 300$ K). The EMD simulation is carried out with the conventional constant number of molecules–volume–temperature (NVT) ensemble. The equations of motion are solved using the velocity Verlet algorithm with a time step Δt under periodic boundary conditions (PBC). The use of PBC is a very practical way to eliminate surface effects from the system. Therefore, a small sample size (micro- or nano-scale) means that, unless surface effects are of particular interest, PBC need to be used [11–13].

Table 1 Simulation parameters

	Variables	Parameters
Xe–Xe	ε_{Xe}	3.12×10^{-21} J
	σ_{Xe}	4.43×10^{-10} m
	m_{Xe}	2.18×10^{-25} kg
	α_{Xe}	14.55
He–He	ε_{He}	1.35×10^{-22} J
	σ_{He}	3.08×10^{-10} m
	m_{He}	6.65×10^{-27} kg
	α_{He}	12.55
Xe–He	ε_{XeHe}	$\sqrt{\varepsilon_{Xe}\varepsilon_{He}}$
	σ_{XeHe}	$\frac{1}{2}(\sigma_{Xe} + \sigma_{He})$
	α_{XeHe}	$\sqrt{\alpha_{Xe}\alpha_{He}}$

The intermolecular potentials of He–He, Xe–Xe, and He–Xe at high pressure (up to 30 GPa) are represented by the exponential-6 intermolecular potential [8];

$$\phi(r) = \frac{\varepsilon}{(\alpha - 6)} \left\{ 6 \exp\left[\alpha\left(1 - \frac{r}{\sigma}\right)\right] - \alpha\left(\frac{\sigma}{r}\right)^6 \right\} \tag{1}$$

where r is the distance between two atoms, ε is the well depth, σ is the separation at the minimum of the well, and α is a parameter that governs the stiffness of the repulsive wall. The values of the parameters for He–He and Xe–Xe in the solid phase are determined using experimental data [8]. The parameters for the He–Xe potential are obtained using Lorentz–Berthelot rules. Table 1 gives the selected parameters. In this article, the potential cut-off radius is 2.5σ.

The EMD-GK simulation employs the fluctuation–dissipation theorem to compute the superlattice thermal conductivity. EMD simulation relies on relating the equilibrium current–current autocorrelation function to the thermal conductivity via the static Green–Kubo expression,

$$\lambda_{\mu\nu} = \frac{1}{V k_B T^2} \int_0^\infty \left\langle J_\mu(0) \cdot J_\nu(t) \right\rangle \mathrm{d}t \tag{2}$$

where V is the volume, k_B is the Boltzmann constant, T is the temperature, J_μ is the μ component of the heat current $\vec{J}(t)$, $\lambda_{\mu\nu}$ is an element of the thermal conductivity tensor, and the angular brackets $\langle\,\rangle$ denote a temporal average. The term inside the angle brackets $\langle J_\mu(0) \cdot J_\nu(t) \rangle$ represents the heat current autocorrelation function (HCACF). The temporal decay of the average HCACF represents the time scale of thermal transport. The thermal conductivity along the three Cartesian directions ($\zeta = x, y, z$) can be computed by setting $\mu = \nu = \zeta$. The ζ component of thermal conductivity λ_ζ is expressed by

$$\lambda_\zeta = \frac{1}{V k_B T^2} \int_0^\infty \left\langle J_\zeta(0) \cdot J_\zeta(t) \right\rangle \mathrm{d}t \tag{3}$$

The heat current $\vec{J}(t)$ is given by

$$\vec{J}(t) = \sum_i \vec{u}_i E_i + \frac{1}{2} \sum_{i,j,i\neq j} \vec{r}_{ij} \left(\vec{f}_{ij} \cdot \vec{u}_i \right) \tag{4}$$

where $\vec{u}_i$ is the velocity of particle i, $\vec{r}_{ij}$ is the relative position vector of atom i and j, $\vec{f}_{ij}$ is the force on atom i due to its neighbor j from the pair potential, and E_i is the "local" energy and is given by

$$E_i = \frac{1}{2} m_i \vec{u}_i^{\,2} + \frac{1}{2} \sum_j \phi\left(\vec{r}_{ij}\right) \tag{5}$$

where m_i is the mass of atom i. In this article, the instantaneous temperature can be obtained from the classical Boltzmann statistical method:

$$\frac{1}{2} \sum_{i=1}^{N} m_i \vec{u}_i^{\,2} = \frac{3}{2} N_\mathrm{a} k_\mathrm{B} T \tag{6}$$

where N_a is the number of atoms.

In fact, the ζ component ($\zeta = x, y, z$) of thermal conductivity λ_ζ is calculated by discretizing the right-hand side of Eq. 3 in EMD time steps Δt as

$$\lambda_\zeta = \frac{\Delta t}{V k_\mathrm{B} T^2} \sum_{m=1}^{M} \frac{1}{N-m} \sum_{n=1}^{N-m} J_\zeta(m+n) J_\zeta(n) \tag{7}$$

where N is the number of EMD steps after equilibration, M is the number of steps over which the time average is calculated, and $J_\zeta(m+n)$ is the heat current at EMD time step $m+n$. In an EMD simulation, calculations are performed with 10^6 MD steps (namely, $N_f = 10^6$) of length $\Delta t = 2\,\mathrm{fs}$ until the data runs are about 2.0 ns. Another two levels of time steps are exercised: $N = 0.9N_f$, $M = 0.01N_f$. The lattice constant is dependent on the density and the number of atoms in the system.

3 Molecular Structure of the Superlattices

3.1 Molecular Structure of $Xe(He)_2$ Superlattices of Nanocrystal

For the stoichiometric solid structure $Xe(He)_2$, it is assumed that $Xe(He)_2$ has the same AB_2 structure as for Murray and Sanders [2,8,14]: the Xe atoms form close-packed hexagonal layers and are in position (0,0,0) of the hexagonal unit cell, whereas the He atoms are in positions (2/3, l/3, l/3) and (l/3, 2/3, l/3) of the hexagonal unit cell and form planar hexagonal layers that alternate with the Xe layers, two Xe atoms sitting above and below the centers of the He rings, respectively. As the characteristic parameter of the hexagonal unit cell, the ratio of c/a is close to 1.04 (c is the height

of the hexagonal cell; a is the length of the hexagonal side). The $Xe(He)_2$ hexagonal unit cell and superlattices have been shown in Fig. 1a–c.

3.2 Molecular Structure of $Xe(He)_{13}$ Superlattices of Nanocrystal

For the stoichiometric solid structure $Xe(He)_{13}$, it is assumed that $Xe(He)_{13}$ has the same AB_{13} structure as observed by Murray and Sanders [2,8,14]: the Xe atoms sit on the corners of the cubic unit cell in position (0,0,0), whereas one He atom sits at the center of the cube at position (l/2, 1/2, 1/2) and the other 12 He atoms are in positions $(1/2 + a, 1/2 + b, 1/2 + c)$ where one of the three parameters (a, b, c) is equal to zero, the remaining two having equal moduli, but not necessarily the same sign. These positions are the corners of a cuboctahedron, which has six square sides parallel to the sides of the cubic unit cell, and eight triangular sides perpendicular to the body diagonals of the cubic unit cell. As the characteristic parameter of the above unit cell, the ratio $2r/d$ is close to 0.59 (r is the cuboctahedron radius; d is the side of the cubic unit cell). The $Xe(He)_{13}$ cubic-cuboctahedral unit cell and superlattices are shown in Fig. 2a, b.

4 Results and Discussion

4.1 Validation of the EMD Code

In order to validate the EMD code in this study, the following measures are taken: (1) the pressures are calculated by EMD simulation and are compared with those from Ref. [8]; and (2) the thermal conductivities are obtained from NEMD and EMD and are compared with each other. Sections 4.1.1 and 4.1.2 briefly describe the methods for calculating pressures and thermal conductivities using EMD or NEMD.

4.1.1 Calculation of Pressure in EMD Simulation

In the EMD simulation, the complete expression for the pressure is given by [15]

$$P = \frac{N_a k_B T}{V} + \frac{1}{3V} \sum_{i,j,i\neq j} \left(\vec{f}_{ij} \cdot \vec{r}_{ij} \right) \tag{8}$$

where P is the pressure.

4.1.2 Calculation of Thermal Conductivity in NEMD Simulation

NEMD simulation will rely on the so-called direct method, i.e., calculate the thermal conductivity from the temperature gradient and heat flux. The ζcomponent ($\zeta = x, y, z$) of thermal conductivity λ_ζ is calculated based on Fourier's law:

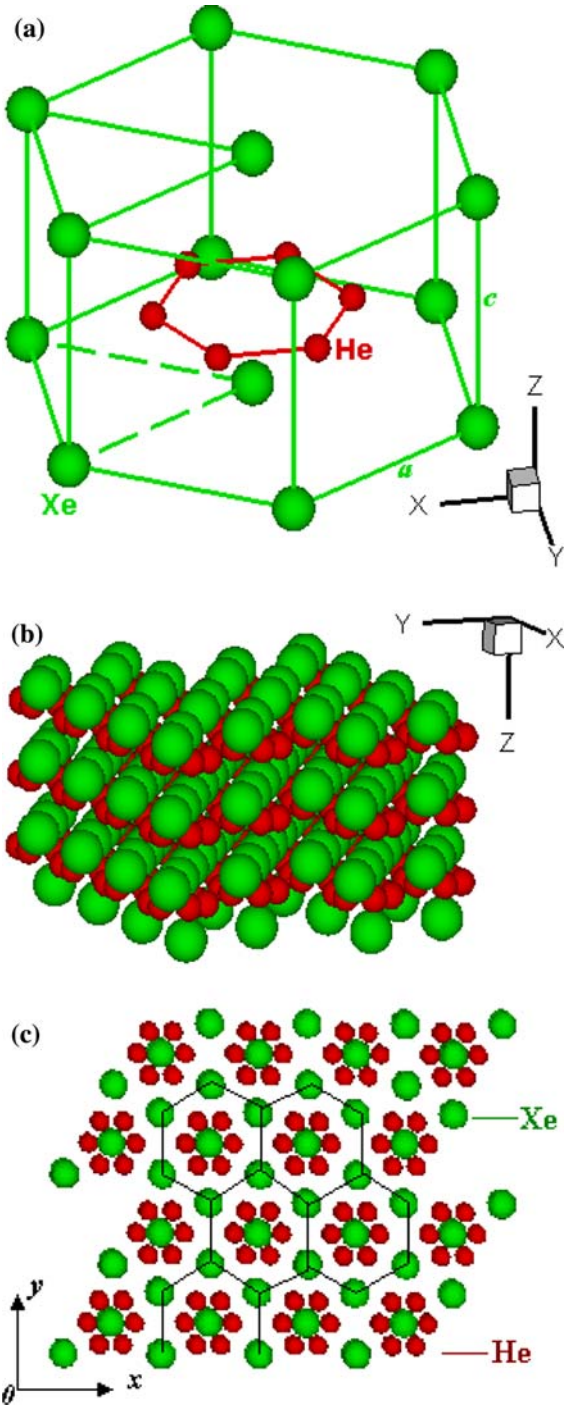

Fig. 1 (**a**) Hexagonal $Xe(He)_2$ unit cell; (**b**) $Xe(He)_2$ superlattices; and (**c**) observed plane from *top*

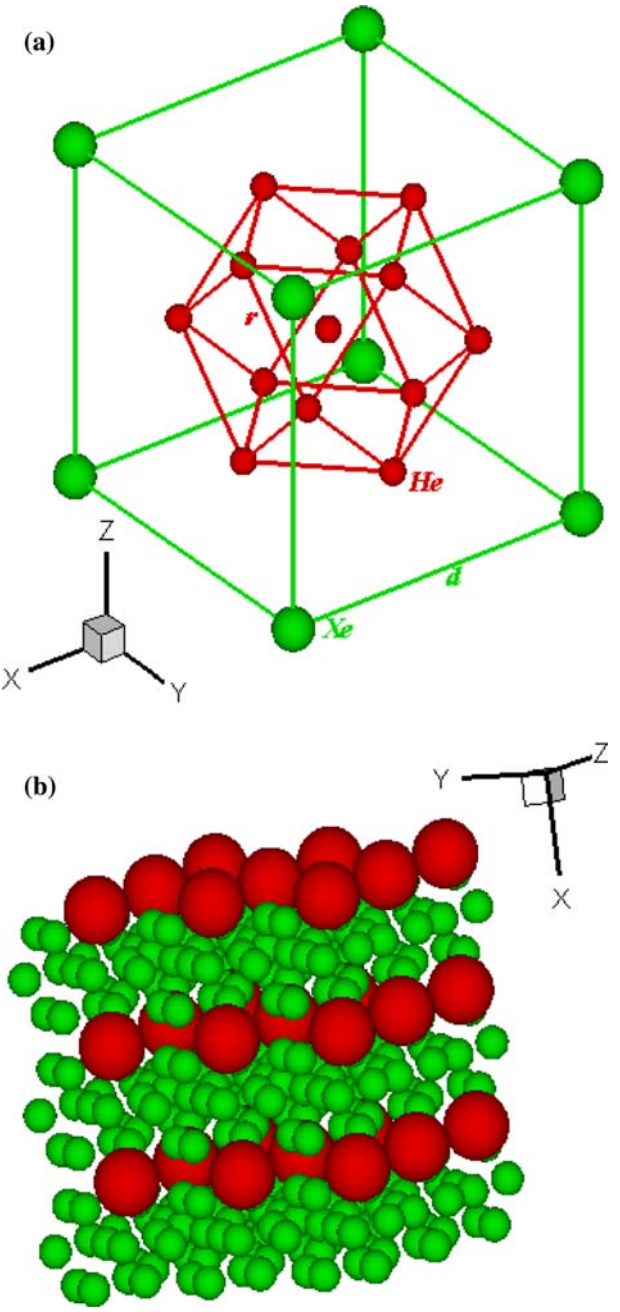

Fig. 2 (**a**) Cuboctahedral $Xe(He)_{13}$ unit cell and (**b**) $Xe(He)_{13}$ superlattices

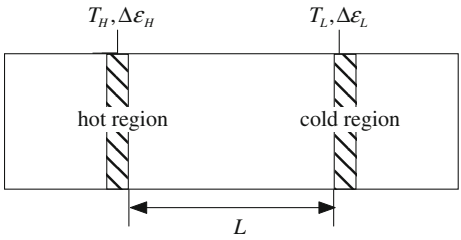

Fig. 3 Schematic region of adding or removing kinetic energy under PBC

$$\lambda_\zeta = -\frac{J'_\zeta}{\partial T/\partial\zeta} \tag{9}$$

J'_ζ is the heat flux per unit area and is parallel to the gradient of the temperature T.

In this NEMD simulation, the constant temperature gradient method is employed to calculate the thermal conductivity. Using a well-equilibrated sample, the two regions are coupled with Berendsen thermostats locally, and each region is set to remain at a constant temperature. Elsewhere, the dynamics were pure Newtonian. This is schematically shown in Fig. 3. PBC were used in all the directions. The system reaches a stationary state due to its thermal conductivity. The energy creation rate $\Delta\varepsilon_\mathrm{H}$ and the energy removal rate $\Delta\varepsilon_\mathrm{L}$ can be calculated. In each time step, the energy change rate $\Delta\varepsilon_\eta$ is given by [16]

$$\Delta\varepsilon_\eta = \sum_i^{N_\eta}\left[\frac{1}{2}m_i\vec{u}^2_{i,\mathrm{old}}\left(\frac{T_\mathrm{t}}{T_\mathrm{c}}-1\right)\right], \quad (\eta = \mathrm{H,L}) \tag{10}$$

where the sum extends over the N_H atoms i in the hot region and N_L atoms i in the cold region. $\vec{u}_{i,\mathrm{old}}$ is the velocity before rescaling. T_t and T_c are the target and current temperatures, respectively. Thus, the heat flux per unit area energy J'_ζ is $J'_\zeta = \Delta\varepsilon_\gamma/(2A\Delta t)$, where A is the interface area of the sample perpendicular to the heat flux, Δt is the time step, and γ = H or L. The factor two is to account for splitting this energy into two fluxes because of the periodic boundary.

The thermal conductivity λ_ζ is obtained from the above calculations as

$$\lambda_\zeta = -\frac{\langle\Delta\varepsilon/\Delta t\rangle}{2A\,\langle\partial T/\partial\zeta\rangle} = \frac{\langle|\Delta\varepsilon/\Delta t|\rangle}{2A\,\langle|(T_\mathrm{H}-T_\mathrm{L})/L|\rangle} \tag{11}$$

where L is the distance between the hot region and cold region and the angular brackets $\langle\,\rangle$ denote a temporal average.

Initially, the system maintains the temperature $T = 300$ K and relaxes for 10^6 MD steps of length $\Delta t = 2$ fs, which puts the system in an equilibrium state. And then the temperature in the thermostated regions are set to $T_\mathrm{H} = 310$ K and $T_\mathrm{L} = 290$ K, and each region is set to remain at a constant temperature. The coupling time of the local Berendsen thermostat in each region is 0.1 ps to keep the average temperature within 0.3 K of the target temperature.

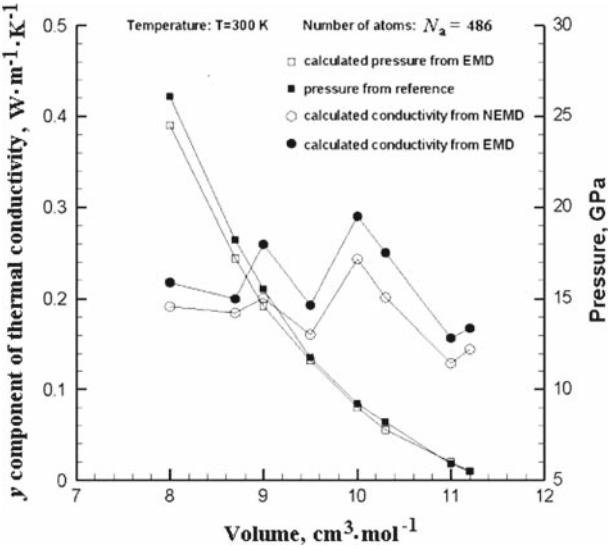

Fig. 4 Comparison of the pressure and thermal conductivity of a $Xe(He)_2$ compound

4.1.3 Comparison of Simulation Results

The $Xe(He)_2$ compound with a $3 \times 6 \times 3$ unit cell (atomic number is 486) is selected as the simulation system. The simulation system volume depends on its molar volume at constant atomic number. The pressure of the simulation system is calculated using an EMD simulation and is compared with that from Ref. [8] in Fig. 4. The y components of thermal conductivities λ_y are obtained from NEMD and EMD and are also shown in Fig. 4. Figure 4 shows that the EMD simulation in this study confirms the great reliability in predicting thermodynamic properties such as pressure and conductivity. The pressures obtained agree very well with those from the reference, to within 5 %. The thermal conductivities calculated by EMD are on the same order of magnitude as the results calculated by NEMD.

Figure 4 also shows that thermal conductivities predicted by both EMD and NEMD are dependent on the system's molar volume and show oscillations. This oscillation behavior mainly results from the finite-size effects because "Both methods (EMD-GK and NEMD) exhibit finite-size effects [12]." The finite-size effects permit the thermal conductivity in the small size systems to depend on the system size. This size dependence of thermal conductivity usually results in oscillations with the variation of system size; the size dependence is also called the "period length dependence" in a periodic structure such as a superlattice. It should be noted that the oscillation behavior of thermal conductivities might partly arise from the round-off errors in MD simulation. As an alternative result of the finite-size effects, the thermal conductivities obtained from NEMD are smaller than those from EMD-GK (as shown in Fig. 4), because the finite size in the NEMD simulation may permit the boundary conditions to affect the phonon distribution, leading to false temperature gradients in the vicinity of the interfaces. In other words, phonon scattering at the hot and cold bath bound-

aries may lead to a shorter phonon mean free path and smaller thermal conductivity. Finite-size effects and the role of phonon scattering in thermal conductivity will be briefly discussed in the following section.

4.2 Discussion

To investigate the effect factor on the anisotropic thermal conductivities of the helium–xenon BNSLs, EMD simulation is used to predict the anisotropic thermal conductivities of helium–xenon BNSLs which have different molar volumes, different number of atoms, and different molecular structures (e.g., the stoichiometric solid structures $Xe(He)_2$ and $Xe(He)_{13}$), all at room temperature ($T = 300\,K$). Table 2 reports all the calculated results including the thermal conductivities of three directions and their averaged values.

4.2.1 Effect of Molecular Structure

From Table 2, both the magnitude and anisotropy of thermal conductivity are significantly dependent on the molecular structure. For example, Table 2 shows that the average thermal conductivities of the stoichiometric solid structure $Xe(He)_{13}$ (samples 10–18) around are more than ten times those of the stoichiometric solid structure $Xe(He)_2$ (samples 1–9), e.g., the ratio of λ_{avr} of sample 18 to λ_{avr} of sample 9 = 2.9101/0.2358 = 12.34. Table 2 also shows that the thermal conductivities of $Xe(He)_2$ are more strongly anisotropic than those of $Xe(He)_{13}$, as the anisotropic factors of the thermal conductivities of $Xe(He)_2$ (expect for sample 6) all are more than 2.0, whereas those of $Xe(He)_{13}$ (expect for sample 17) all are less than 2.0. According to the definition of the anisotropic factor (see Table 2), the anisotropic factor is equal to 1.0 when the thermal conductivity is isotropic. The above phenomenon is caused by the helium–xenon BNSLs with different compound concentrations and the symmetries of a unit cell. MD simulation is a convenient tool for modeling and prediction since it allows determination of the temperature, lattice parameter, and precise specification of compound (or impurity) concentration.

In order to understand the thermal-conductivity trends (the thermal conductivities of $Xe(He)_{13}$ are larger then those of $Xe(He)_2$ in magnitude while they are less anisotropic than those of $Xe(He)_{2)}$, one must consider the effects of molecular structure, with consideration to the molecular composition and topology (e.g., the mass and arrangement of atoms in a molecule). Since the BNSLs studied here are all nonmetallic and there are no free electrons to carry the heat, the heat transport depends predominantly on the phonons (lattice vibrations). The phonon relaxation time approach, describing the phonon scattering process, is usually utilized to understand the heat transport mechanism. The phonon relaxation time is determined from the temporal decay of the autocorrelation function (ACF) of the phonons' energy components [17,18]. According to Eq. 3, at a constant volume and temperature, the lattice thermal conductivity increases as the phonon relaxation time (the mean free time in phonon scattering) increases. The above relationship that the thermal conductivity is proportional to the phonon mean free path (or the phonon relaxation time) also can be deduced from the phonon kinetic theory

Table 2 Thermal conductivities of three directions and their average values

Compound	Dimensions (Unit cell)	Number of atoms	Sample number	Molar volume ($cm^3 \cdot mol^{-1}$)	λ_x ($W \cdot m^{-1} \cdot K^{-1}$)	λ_y ($W \cdot m^{-1} \cdot K^{-1}$)	λ_z ($W \cdot m^{-1} \cdot K^{-1}$)	λ_{avr} ($W \cdot m^{-1} \cdot K^{-1}$)	Anisotropic factor
$Xe(He)_2$	$3 \times 3 \times 3$	243	1	10.3	0.2544	0.3541	0.0925	0.2337	3.83
			2	11.0	0.2745	0.2609	0.0948	0.2101	2.90
			3	11.2	0.3540	0.2753	0.1588	0.2627	2.23
	$3 \times 3 \times 4$	324	4	10.3	0.2516	0.1134	0.0138	0.1262	18.2
			5	11.0	0.1737	0.1079	0.0491	0.1102	3.54
			6	11.2	0.2595	0.1347	0.1327	0.1756	1.96
	$4 \times 5 \times 5$	900	7	10.3	0.3844	0.3760	0.1662	0.3089	2.31
			8	11.0	0.2582	0.4574	0.1601	0.2919	2.86
			9	11.2	0.3418	0.2376	0.1281	0.2358	2.67
$Xe(He)_{13}$	$3 \times 3 \times 3$	378	10	10.3	3.5663	3.3565	1.9582	2.9604	1.82
			11	11.0	2.9912	2.8918	3.0757	2.9862	1.06
			12	11.2	2.8465	2.2485	2.8185	2.6378	1.26
	$3 \times 3 \times 4$	504	13	10.3	2.4022	4.1271	2.9929	3.1740	1.72
			14	11.0	2.4564	3.8576	2.9595	3.0912	1.57
			15	11.2	1.4548	2.1606	2.6300	2.0818	1.81
	$4 \times 4 \times 4$	896	16	10.3	2.8964	2.6034	3.0176	2.8391	1.16
			17	11.0	2.9165	1.7249	3.9432	2.8615	2.29
			18	11.2	3.2530	3.1993	2.2782	2.9101	1.43

Note: Anisotropic factor = (the maximum of λ_x, λ_y, and λ_z)/(the minimum of λ_x, λ_y, and λ_z)

or a Boltzmann phonon transport equation (BPTE) incorporating the different phonon models (e.g., Debye model) [19], where the phonon mean free path is proportional to the phonon relaxation time. However, exact or even numerical predictions of the thermal conductivity from BPTE is a formidable task due to the complexity of the BPTE, while it is also impossible to expect a quantitatively accurate thermal conductivity from the phonon kinetic theory based on some over-simplified assumptions.

The Callaway model, which includes phonon-surface diffusive scattering τ_s^{-1}, phonon–electron scattering τ_e^{-1}, phonon–phonon (normal and umklapp) scattering τ_p^{-1}, and phonon–defect scattering τ_d^{-1}, is employed to express the total relaxation time of phonon τ according to Matthiessens' rule: $\tau^{-1} = \sum_i \tau_i^{-1} = \tau_s^{-1} + \tau_e^{-1} + \tau_p^{-1} + \tau_d^{-1}$, where τ is the relaxation time, τ^{-1} is the scattering rate (reciprocal relaxation time), and τ_i^{-1} represents the individual phonon scattering processes. Thus, τ_s^{-1} is not considered due to the PBC used in this study (EMD-GK), and τ_e^{-1} also is not considered, as no free electrons exist in the BNSLs studied here. Phonon–phonon scattering includes two kinds of scattering: normal scattering $\tau_{p,n}^{-1}$ and umklapp scattering $\tau_{p,u}^{-1}$ where phonon–phonon scattering $\tau_p^{-1} = \tau_{p,n}^{-1} + \tau_{p,u}^{-1} = (B_1 + B_2)\omega^2 T^3$, which can be treated as a constant for a given sample with a constant temperature. Defect scattering arises from imperfections in the crystal and scatters phonons by local alternation of strain and mass density. The point defect scattering rate τ_d^{-1} is taken from the mass effects plus strain effects [20]:

$$\tau_d^{-1} = \tau_{ma}^{-1} + \tau_{st}^{-1}, \quad \tau_{ma}^{-1} = C_{ma} \sum_k f_k \left(1 - \frac{m_k}{m_{av}}\right)^2,$$
$$\tau_{st}^{-1} = C_{st} \sum_k f_k \left(1 - \frac{R_k}{R}\right)^2, \tag{12}$$

where C_{ma} and C_{st} are the mass and distance independence of the expressions, R_k and R indicate the radii of the impurity and host atoms, respectively, f_k is the atomic fraction of a component k, m_k is the atomic mass of species k, and m_{av} is the average mass of all the atoms, including impurities. To sum up the above analysis, at constant temperature, in order to qualitatively compare the phonon relaxation time of samples with different impurities, only defect scattering, which is related to molecular structure (e.g., the mass and arrangement of atoms in a molecule), needs to be compared. Some detailed descriptions of the phonon-scattering mechanisms are provided in Refs. [19–22].

Now we turn to a brief discussion of the phenomenon that the thermal conductivities of $Xe(He)_{13}$ are larger then those of $Xe(He)_2$ in magnitude, assuming that atomic Xe is an impurity in helium–xenon BNSLs. The following results can be obtained from Eq. 12: $\tau_{ma,Xe(He)_2}^{-1}/\tau_{ma,Xe(He)_{13}}^{-1} = (336.55 C_{ma})/(72.12 C_{ma}) = 4.67$; and $\tau_{st,Xe(He)_2}^{-1}/\tau_{st,Xe(He)_{13}}^{-1} = (9.15 \times 10^{-2} C_{st})/(1.56 \times 10^{-2} C_{st}) = 5.85$; and then $\tau_{d,Xe(He)_2}^{-1} = \tau_{ma,Xe(He)_2}^{-1} + \tau_{st,Xe(He)_2}^{-1}$ is larger than $\tau_{d,Xe(He)_{13}}^{-1} = \tau_{ma,Xe(He)_{13}}^{-1} + \tau_{st,Xe(He)_{13}}^{-1}$, where $\tau_{ma,Xe(He)_2}^{-1}$, $\tau_{st,Xe(He)_2}^{-1}$, $\tau_{d,Xe(He)_2}^{-1}$ are, respectively, the mass-defect scattering rate, the

strain-defect scattering rate, and defect scattering rate in the $Xe(He)_2$-type BNSL. $\tau^{-1}_{ma,Xe(He)_2}$, $\tau^{-1}_{st,Xe(He)_2}$, $\tau^{-1}_{d,Xe(He)_2}$ denote the corresponding parameters of the $Xe(He)_{13}$-type BNSL. For values of the above parameters, see Sect. 3 and Table 1. $\tau^{-1}_{d,Xe(He)_2} > \tau^{-1}_{d,Xe(He)_{13}}$ means $\tau_{d,Xe(He)_2} < \tau_{d,Xe(He)_{13}}$ indicating that the thermal conductivities of $Xe(He)_{13}$ are larger then those of $Xe(He)_2$ in magnitude because the phonon relaxation time in $Xe(He)_{13}$ is longer than that in $Xe(He)_2$.

As far as the phenomenon that $Xe(He)_2$ is stronger than $Xe(He)_{13}$ in the anisotropy of thermal conductivities, it can be explained by the molecular structure of BNSLs (e.g., the arrangement of atoms in a molecule). Because phonon velocity anisotropy is related to the crystal (molecular) symmetry most usually defined by the shape of the unit cell, this indicates stronger anisotropy for crystals with lower symmetry [23]. The $Xe(He)_2$ unit cell consists of a simple hexagonal arrangement of large Xe particles, with the smaller He particles filling all the interstices between the Xe layers (honeycomb pattern). Hexagonal symmetry occurs in the unit cell with the form of a hexagonal prism, where there are six axes of symmetry in one plane, and a further axis at 90° to the other three. So the $Xe(He)_2$-type BNSL has six mirror planes and one axis of rotational symmetry. However, the $Xe(He)_{13}$ unit cell consists of a simple cubic lattice of large Xe spheres with a regular cuboctahedron cluster of 13 He particles in the body-center of each unit cell. A regular cuboctahedron belongs to the FCC packing arrangement. The FCC cuboctahedron cluster is demonstrated to possess four intersecting layers that correspond to the four (111) planes of cubic symmetry. In consequence, the $Xe(He)_{13}$-type BNSL (cubic containing a FCC cuboctahedron cluster in each unit cell) possesses full cubic symmetry with nine mirror planes and seven axes of rotational symmetry. That means that the $Xe(He)_{13}$-type BNSL is more symmetrical than the $Xe(He)_2$-type BNSL. Therefore, $Xe(He)_2$ is stronger than $Xe(He)_{13}$ in anisotropy of thermal conductivities.

4.2.2 Finite-Size Effects

Calculated data in Table 2 also show that both the magnitude and anisotropy of thermal conductivities of helium–xenon BNSLs ($Xe(He)_2$ and $Xe(He)_{13}$) are slightly dependent on the molar volume and atomic number of the simulation system. Thus, the size dependence of the thermal conductivity possibly results from the finite-size effects in the small MD simulation. In this study, at room temperature, the phonon mean free path is in the range 1 nm to 100 nm, which is comparable to the size of BNSLs. In fact, finite-size effects arise when the simulation domain length is not significantly longer than the phonon mean free path. The key factors generating size artifacts in an MD simulation are the frequency cutoff imposed by the simulation domain length and the correlation artifacts caused by the PBC. The frequency cutoff results in the following two consequences: (1) the contribution of low-frequency phonons to the thermal conductivity is excluded; and (2) the static disturbance values are not allowed at all in the simulation domain. As far as the correlation artifacts caused by the PBC, it can be explained using an example. For the case of small size systems with the PBC, a phonon may pass the same point in space several times without scattering. However, the system may retain some dynamical information during the passage of the phonon, so artificial correlations may be introduced in the autocorrelation function. A more

detailed discussion of finite-size effects in MD simulations can be found elsewhere [10,12].

5 Conclusions

The anisotropic thermal conductivities of helium–xenon BNSLs are calculated via EMD simulation. Simulation has been carried out on stoichiometric solid structures ($Xe(He)_2$ and $Xe(He)_{13}$) with different molar volumes and atomic numbers. Results show that the thermal conductivities of $Xe(He)_2$ are more strongly anisotropic than those of $Xe(He)_{13}$, whereas the average thermal conductivities of $Xe(He)_2$ are about one tenth (1/10) of those of $Xe(He)_{13}$, indicating that the thermal conductivities of helium–xenon BNSLs ($Xe(He)_2$ and $Xe(He)_{13}$) significantly depend on the molecular structure in both magnitude and anisotropy. The results also show that both the magnitude and anisotropy of the thermal conductivity of helium–xenon BNSLs ($Xe(He)_2$ and $Xe(He)_{13}$) depend slightly on the atomic number and molar volume of the simulation system, with finite-size effects existing in nanoscale systems.

References

1. J.V. Sanders, Philos. Mag. A **42**, 705 (1980)
2. M.J. Murray, J.V. Sanders, Philos. Mag. A **42**, 721 (1980)
3. E.V. Shevchenko, D.V. Talapin, A.L. Rogach, A. Kornowski, M. Haase, H. Weller, J. Am. Chem. Soc. **124**, 11480 (2002)
4. F.X. Redl, K.-S. Cho, C.B. Murray, S. O'Brien, Nature **423**, 968 (2003)
5. E.V. Shevchenko, D.V. Talapin, C.B. Murray, S. O'Brien, J. Am. Chem. Soc. **128**, 3620 (2006)
6. T.D. Ewers, A.K. Sra, Q. Xu, H. Zandbergenb, R.E. Schaak, Chem. Commun. (2006). doi:10.1039/b515673d
7. D.J. Evans, G.P. Morriss, Comput. Phys. Rep. **1**, 297 (1984)
8. J.-L. Barrat, W.L. Vos, J. Chem. Phys. **8**, 5707 (1997)
9. A.N. Bodapati, *Structural Disorder and Thermal Transport in Nanoscale Solids*, Dissertation, Rensselaer Polytechnic Institute, 2006, available via DIALOG, http://proquest.calis.edu.cn, cited 15 Dec 2008
10. S.G. Volz, G. Chen, Phys. Rev. B **61**, 2651(2000)
11. M.P. Allen, *Introduction to Molecular Dynamics Simulation* (University of Warwick, UK, 2004), available via DIALOG, http://www.fz-juelich.de/nic-series/volume23/allen.pdf, cited 15 Dec 2008
12. P.K. Schelling, S.R. Phillpot, P. Keblinski, Phys. Rev. B **65**, 144306 (2002)
13. T. Sirk, *Numerical Simulation of Nanoscale Flow: A Molecular Dynamics Study of Drag*, Thesis, Virginia Polytechnic Institute and State University, Blacksburg, VA, 2006, available via DIALOG, http://scholar.lib.vt.edu/theses/available/etd-05042006-190812/unrestricted/SIRK.pdf, cited 15 Dec 2008
14. A.B. Schofield, P.N. Pusey, P. Radcliffe, Phys. Rev. E **72**, 031407 (2005)
15. N. Ogbonna, *Molecular Dynamics Simulation*, Post-graduate Diploma Essay, African Institute for Mathematical Sciences, South Africa, 2004, available via DIALOG, http://users.aims.ac.za/~nneoma/theses/NneomaAimsEssay.pdf, cited 15 Dec 2008
16. S.-H. Choi, S. Maruyama, Int. J. Therm. Sci. **44**, 547 (2005)
17. A.J.H. McGaughey, M. Kaviany, Phys. Rev. B **69**, 094303 (2004)
18. A. Ladd, B. Moran, W.G. Hoover, Phys. Rev. B **34**, 5058 (1986)
19. W.C.W. Fon, *Thermal Properties of Nano- and Microstructures*, Dissertation, California Institute of Technology, Pasadena, CA, 2004, available via DIALOG, http://etd.caltech.edu/etd/available/etd-05262004-123035/unrestricted/Thesis.pdf, cited 15 Dec 2008
20. Y. Chen, J.R. Lukes, J. Yang, Y. Wu, J. Chem. Phys. **120**, 3841 (2004)

21. Y. Hudiono, *Thermal Transport Properties of Nanoporous Zeolite Thin Films*, Dissertation, Georgia Institute of Technology, Atlanta, GA, 2008, available via DIALOG, http://etd.gatech.edu/theses/available/etd-07032008-122258/unrestricted/Hudiono_yeny_200808_phd.pdf, cited 15 Dec 2008
22. J.D. Chung, A.J.H. McGaughey, M. Kaviany, ASME J. Heat Transfer (2004). doi:10.1115/1.1723469
23. I. Soroka, *Magnetic Heterostructures*: *The Effect of Compositional Modulation on Magnetic Properties*, Dissertation, Uppsala University, Sweden, 2005, available via DIALOG, http://www.diva-portal.org/diva/getDocument?urn_nbn_se_uu_diva-5733-2__fulltext.pdf, cited 15 Dec 2008